NISTIR 5670

Change Detection Algorithm for Machine Vision Applications

Sridhar R. Kundur
Robotics Center and
Department of Electrical Engineering
Florida Atlantic University
Boca Raton, FL 33431

and

Daniel Raviv
Robotics Center and
Department of Electrical Engineering
Florida Atlantic University
Boca Raton, FL 33431
and Intelligent Systems Division

U.S. DEPARTMENT OF COMMERCE
Technology Administration
National Institute of Standards
and Technology
Bldg. 220 Rm. B124
Gaithersburg, MD 20899

NIST

NISTIR 5670

Change Detection Algorithm for Machine Vision Applications

Sridhar R. Kundur
Robotics Center and
Department of Electrical Engineering
Florida Atlantic University
Boca Raton, FL 33431

and

Daniel Raviv
Robotics Center and
Department of Electrical Engineering
Florida Atlantic University
Boca Raton, FL 33431
and Intelligent Systems Division

U.S. DEPARTMENT OF COMMERCE
Technology Administration
National Institute of Standards
and Technology
Bldg. 220 Rm. B124
Gaithersburg, MD 20899

June 1995

U.S. DEPARTMENT OF COMMERCE
Ronald H. Brown, Secretary

TECHNOLOGY ADMINISTRATION
Mary L. Good, Under Secretary for Technology

NATIONAL INSTITUTE OF STANDARDS
AND TECHNOLOGY
Arati Prabhakar, Director

Change Detection Algorithm for Machine Vision Applications*

Sridhar R. Kundur[1] and Daniel Raviv[1,2]
[1]*Robotics Center and Department of Electrical Engineering*
Florida Atlantic University, Boca Raton, FL 33431
[2]*Intelligent Systems Division,*
National Institute of Standards and Technology(NIST)
Bldg. 220, Room B124, Gaithersburg, MD 20899
email: kundur@acc.fau.edu and ravivd@acc.fau.edu

Abstract

Detection of changes from one image to another play an important role in many machine vision applications such as visual monitoring of events, triggering of events based on changes in images, etc. This paper presents a new approach for detecting changes from one image to another without any *a-priori* knowledge about the 3D scene or the camera parameters. The approach is based on a global measure for image dissimilarity, we call the DisSimilarity Measure (DSM). Based on the variations in the DSM value in the Region Of Interest (ROI) it is possible to detect changes in the scene under surveillance. The algorithm needs *no preprocessing* and can be extracted *directly from the raw data of the gray level of images*. It is *robust* to small vibrations, where approaches like image differencing may fail. It needs *no feature correspondence* between images and can be used in many environments. It is simple and is suitable for parallel hardware implementation.

This algorithm was applied to several real, as well as standard synthetic, image sequences where there is a change between one frame and another. The results are highly encouraging. Several potential applications of this change detection algorithm are outlined.

Key Words: Change Detection, Image Dissimilarity, Visual Surveillance, Machine Vision

---

* This work was supported in part by a grant from the National Science Foundation, Division of Information, Robotics and Intelligent Systems, Grant # IRI-9115939

1 Introduction

Detection of changes from one image to another play an important role in visual surveillance of events, triggering of events on the basis of changes in the images, etc.[1-3, 13, 16, 17, 21]. For example, consider the task of generating masks in an image corresponding to moving objects in a scene [2]. Detection of changes from an image sequence is an input parameter in such applications [3]. In flood control applications one is interested in the *variations* in the width of the river and not its actual width. Similarly urban planning is based on the rate at which man-made structures are built or demolished in a city and not on the actual number of buildings in it. Assessment of aforestation or deforestation depends upon the changes in the trees and not on the nature of trees in the forest. Change detection also plays a major role in the area of remote sensing for monitoring variations in patterns of vegetation on land, sea erosion, weather prediction from satellite images and so on. Similarly in many industrial machine vision applications such as picking an object from the conveyor from a certain location and placing it elsewhere depends upon the changes in a particular region of the scene being monitored and not on the type of the object. Encroachment of one country into its neighboring country is partially judged on the basis of changes in the number of tanks and other weaponry at the border between the states. Many other defense applications of change detection are possible (see for example [13]).

Temporal variations in image intensity may be due to many reasons such as relative motion between the scene and the sensor, drifts in illumination due to vibration, noise or disturbance, camera parameters, changes in the scene and so on. The primary objective of

a change detection algorithm is to isolate the changes due to the disturbances. In the following paragraphs we present a brief summary of commonly used change detection algorithms.

Image differencing is one of the conventional approaches employed for detecting changes (see for example [4]). Several modifications of this approach have been employed in which the mean squared difference, mean value, etc., have been used as change detection criteria [5, 6]. These approaches serve as reliable change detectors only if the Signal to Noise Ratio (SNR) is high [7, 8]. The change detection algorithms based on pixel-by-pixel subtraction of images are sensitive to small motion vibrations in the imaging systems, in particular where the field of view is narrow. It is also sensitive to drifts in images due to disturbances like wind (for example if the scene to be monitored is a tree). In Appendix C it is shown that a small shift (1, 2, or 3 pixel shift) in images causes very big changes, which is undesirable.

Several statistical change detection algorithms have been proposed. Parametric-based approaches namely likelihood and sample mean have been employed for detecting changes in images [9]. Various likelihood ratio-based approaches for detecting changes were presented by modeling the image as gaussian processes [10, 11]. Usually the statistical approaches are based on modeling the image data by a white Gaussian process. In other words, some a-priori information about the being imaged is necessary.

In [12] a principal component analysis based algorithm has been employed for detection of changes in land-cover in Landsat Multispectral Scanner (MSS) data. The

eigen-vectors used for the transformation is derived from the covariance matrix of the total pixels in the image. Such an analysis is also shown to be scene dependent.

Recently several other approaches for detecting changes in images have been proposed (see for example [1, 13]). A log likelihood-based similarity measure for two histogram distributions has been employed as a change detection criteria [13]. Several other approaches namely edgel-based, energy-based [15] are also presented as change detectors [13].

This paper presents a new, robust, practical approach for detecting changes from one image to another without any *a-priori* knowledge about the 3D scene or the camera parameters. The approach is based on a global measure for image dissimilarity, we call the DisSimilarity Measure (DSM) for the Region Of Interest (ROI) in the image. Our change detection criterion is the *changes in the DSM value* in the ROI in the image. The algorithm needs no preprocessing such as spatio-temporal smoothing, edge detection, binarization, etc., and can be extracted *directly from the raw data of the gray level images.* It is shown that small image drifts or vibrations cause only a minor change in the DSM value, which is a big advantage over approaches like image subtraction which is sensitive to image drifts (see Appendix C). This approach is simple and is suitable for parallel hardware implementation.

The dissimilarity of gray level intensity in a ROI in the image may be characterized in many different ways. In this paper we describe several such DSMs (Appendix B) such as the dissimilarity based on city block metric [22], Minkowski metric [22], etc. for the ROI

in an image. However due to simplicity we have employed the DSM based on the City Block Metric (Appendix A) through out our analysis.

This paper is organized as follows: in section 2 the DisSimilarity Measure (DSM) is described; section 3 explains how the DSM is used for change detection applications; in section 4 we present the experimental results and analysis of the DSM; section 5 outlines a few applications of the DSM in various fields and in section 6 we present a specific application of the DSM in weather forecasting.

2 Dissimilarity Measure

Local spatial gray tone variations in an image give rise to a visual pattern in the image. These spatial gray level variations are due to the visual characteristics of the 3D scene being imaged, the illumination, the range between the scene and the observer, as well as due to camera parameters like zoom, aperture, resolution, focus, etc. The spatial intensity variations around a pixel in a window can be described by several distance metrics. We developed several measures of gray level intensity dissimilarity for the ROI in the image (Appendix B). These dissimilarity measures are based on the distance metrics such as Minkowski metric, city block metric, etc.(see for example [19, 22]). However due to simplicity we have employed the DSM based on the city block metric as the DSM through out our analysis. Similar experiments can be performed with other metrics presented in Appendix B. The algorithm used to extract the DSM value of a ROI in the image is defined as follows (see Appendix A):

$$DSM = \sum_{x=x_i}^{x_f} \sum_{y=y_i}^{y_f} \sum_{p=-L_c}^{L_c} \sum_{q=-L_r}^{L_r} |I(x,y) - I(x+p, y+q)|$$

where I(x,y) is the intensity at pixel (x,y) and x_i and x_f are the initial and final x-coordinates of the image window, respectively; y_i and y_f are the initial and final y-coordinates of the ROI in the image, respectively, and L_c and L_r are positive integer constants.

3 DSM for Change Detection

The DSM described earlier can be used as a measure for detecting temporal changes from one image to another. Consider a scene to be monitored for changes caused due factors other than noise and disturbance (see Figure (1)). These changes may be due to relative motion between the camera, appearance or disappearance of objects in the scene etc. The changes in a scene are reflected by a corresponding change in the DSM value of the ROI in the image. If one constantly monitors the DSM associated with the specific ROI in the image, it would be possible to detect changes in the scene under surveillance. In other words changes in the DSM values can be used as a change detection criteria. We describe two such change detection criteria for the ROI as follows:

a) $\left|\frac{\Delta DSM}{DSM}\right| > Threshold$

b) $|\Delta DSM| > Threshold$

By using the DSM as a change detector one need not save the whole image or image sequence, instead it is sufficient to save one number.

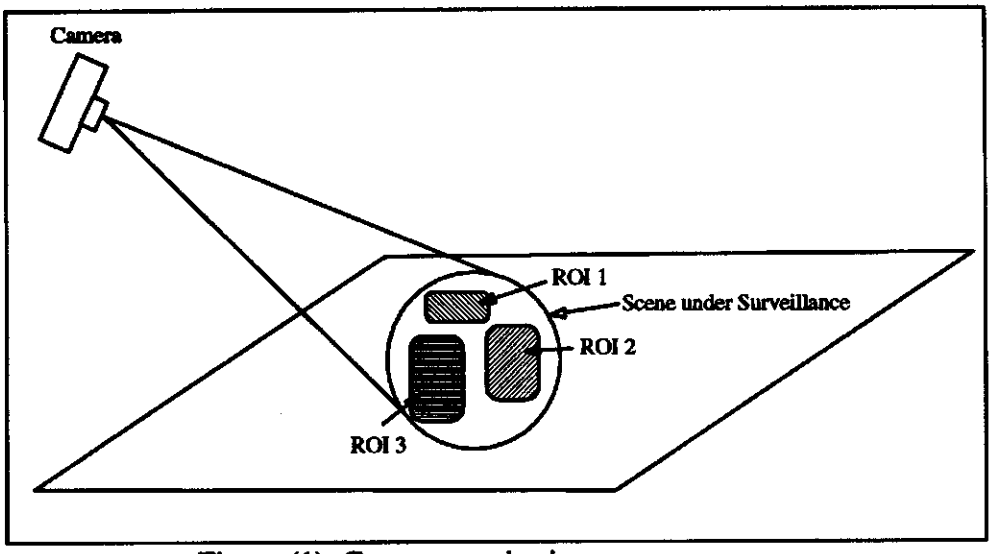

Figure (1): Camera monitoring a scene

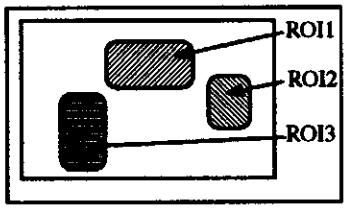

Figure (2): Corresponding image

Some advantages of using the DSM for change detection are:

- It gives a global measure of dissimilarity, i.e., it gives one number for the whole image (or a window in an image) which characterizes the image dissimilarity.
- It does not need any preprocessing, i.e., works directly on the raw gray level data, without any spatial or temporal smoothing, edge detection, binarization, etc.
- It needs no *a-priori* knowledge of the 3-D scene.
- It is simple and handles noise quite robustly.
- It can be implemented on parallel hardware
- Small vibrations in the camera are also tolerated, which is a major advantage over image subtraction approaches (see Appendix C).

4 Experimental Results and Analysis

Several experiments were conducted to test the performance of the change detection algorithm described in the previous section. The DSM described earlier has been employed for detecting changes in images of the same scene where a change has taken place, e.g., appearance/disappearance of aircraft, changes due to motion, etc. The following images have been employed in our analysis:

1. Images of an indoor scene obtained by a CCD camera with and without a miniature aircraft under variations of several parameters like the depth, focus, etc. Figures (3a - 6a), Figures (3b - 6b).
2. The NASA Coke® can sequence [20] (Figure (7a)).
3. The moving square sequence [20] (Figure (8a)).
4. The Hamburg taxi sequence [20] (Figure (9a)).
5. The Yosemite sequence [20] (Figure (10a)).
6. Two satellite pictures obtained from world wide web site of University of Wisconsin (Figure 11).

In Figures 3-6 there are four sets of two images corresponding to images of a scene with and without an aircraft (for example Figures 3a and 3b). The objective is to detect the presence or absence of aircraft in the scene. For each image a DSM value is computed. Note that the DSM is significantly different when an abrupt change (appearance/disappearance of an aircraft) has been introduced. For the given four sets of images (Figures 3-6) these changes vary from 53% (best case, Figure 5) to 29% (worst case, Figure 4). The results are summarized in Table 1. The DSM values presented in this

table have no meaning by themselves, since we are interested in changes from one scene to another. *This shows that if we constantly monitor a 3D scene, the appearance/disappearance of the aircraft (objects) can be detected by observing the deviation in the DSM value.* Note that images in Figures 3-6 are quite noisy.

We tested our algorithm for detecting changes from one image to another in the image sequences namely the Yosemite, the NASA Coke® can, the moving square and the Hamburg taxi sequences described in [20].

Figure (7a) shows nine images of a moving Coke® can sequence (due to space limitations we present only nine images, though we have employed all the images in the image sequence in our testing, also the resolution of the images shown in this paper is about thirty percent lower than the resolution of the original images used in the experiments). Each image in such an image sequence e.g., Figure 7a, is divided into four quadrants namely "top left is quadrant I," "top right is quadrant II," "bottom left is quadrant III" and "bottom right is quadrant IV". The DSM described earlier is evaluated for these quadrants. Since we are interested in the changes in the DSM value and not on its absolute magnitude we normalized the DSM of each quadrant of the sequence by the corresponding maximum value of the DSM for that particular quadrant. Since we are interested in the changes in the DSM value and not its absolute value we present a normalized plot of the DSM (DSM divided by the maximum value of the DSM in the sequence) (Figures 7b). As seen from the plots the variations in the DSM for the four quadrants in the image sequence depict the corresponding variations in the scene.

Similar experiments are performed on the other image sequences namely the moving square sequence (Figure 8), the Hamburg taxi sequence (Figure 9), the Yosemite sequence (Figure 10).

These image sequences namely Figures (7a - 10a) are used for the analysis of optical flow techniques [20], and hence the changes are gradual and in most cases unnoticed by a human user. However they were detected quite consistently by the algorithm.

In the NASA Coke® can sequence (Figure 7a) the changes are not obvious. However if we carefully observe the first and last frame of the sequence we notice that there are some changes in "quadrant III" as well as in "quadrant IV" of the image sequence. In "quadrant III" the distance between the bottom edge of the hole in the flat surface and the bottom edge of the image decreases from the first frame to the last frame. In "quadrant IV" the changes in the images are due to change in positions of the base of the Coke® can as well as the vertical stick. In "quadrant I" as well as "quadrant II" the changes are primarily due to the movement of the Coke® can. These changes in positions of the objects in the scene are reflected in the changes in the corresponding changes in the DSM values. Normalized plots of the DSM values of all the four quadrants as a function of the images in the sequence is shown Figure (7b).

In the moving square sequence (Figure 8a) the square moves from "quadrant III" to "quadrant II" diagonally. The DSM value in "quadrant I" as well as "quadrant IV" increases until a maximum portion of the square is in both the quadrants. Then the DSM value remains almost a constant as long as the area of the square in the quadrants remains the same. It decreases as soon as the area of the square in "quadrant I" and "quadrant IV"

decreases. In "quadrant II" an increase in the DSM value corresponds to the square moving in to that quadrant where as a decrease in the DSM value of "quadrant III" corresponds to the square leaving that quadrant. Normalized plots of the DSM values of all the four quadrants as a function of the images in the sequence is shown Figure (8b).

In the Hamburg taxi sequence (Figure 9a) the relative distance between the two cars in the center of the image increases from the first frame to the last frame mainly due to one car moving away from a stationary one. A major portion of this car in motion is in "quadrant III" in the first frame where as in the last frame a major portion of it is in "quadrant IV". These changes are reflected in the corresponding values of the DSM for "quadrant I" as well as "quadrant III". In other words an increase in the DSM value from the first frame to the last frame of the "quadrant I" corresponds to the car entering the quadrant, while a decrease in the DSM value from the first frame to the last frame corresponds to the car leaving the "quadrant III". Since a small portion of the car in motion is also in "quadrant IV" and as it moves away from this quadrant the DSM value of this quadrant also decreases. The decrease in the DSM value in "quadrant III" is relatively higher than the decrease of the DSM value in the "quadrant IV" because only a small portion of the car is in the "quadrant IV" in the first frame of the sequence. Normalized plots of the DSM values of all the four quadrants as a function of the images in the sequence is shown Figure (8b).

In the Yosemite sequence (Figure 10a) clouds in the upper half of the images are in motion from left to the right. As a result the DSM value of "quadrant I" as well as "quadrant II" increases gradually from the first frame of the sequence to the last one. In

"quadrant III" as well as "quadrant IV" changes in the DSM values are mainly due to relative motion of the sensor from the first frame to the last one. Normalized plots of the DSM values of all the four quadrants as a function of the images in the sequence is shown Figure (10b).

In Figures (7a-10a) only nine images of each sequence are shown due to space limitations although all the images of the sequence are employed in the analysis. Also the images presented in Figures (7a-10a) are of lower resolution (about 25 percent lower resolution than the images used in the analysis) due to limitations on computer memory limitations of this document.

Finally we employed the DSM to detect the presence or absence of clouds in an Infra Red satellite picture of the North America (Figure 11). This is done primarily for illustrating its application in weather monitoring. This algorithm has been applied in ten states of the USA. It is applied to states that are approximately a rectangle and can be extended to states of different geometrical shapes. Each state has been divided into four different regions and the DSM value is extracted in all the four regions of the state. The results are summarized in Table 2. Based on the changes in the DSM value of the monitored state, with some a-priori knowledge like the DSM with out any clouds, it may be possible to develop a weather forecasting system..

Figure (3a): Scene with out air-craft
DSM = 193

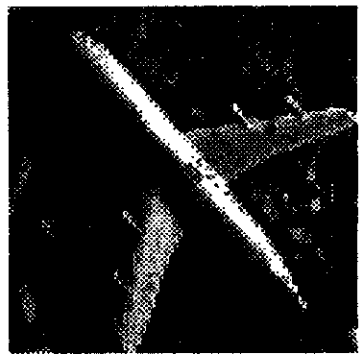

Figure (3b): Same scene of Figure (3a) with air-craft
DSM = 141

Figure (4a): Scene without air-craft
DSM = 195

Figure (4b): Same scene of Figure (4a) with air-craft
DSM = 151

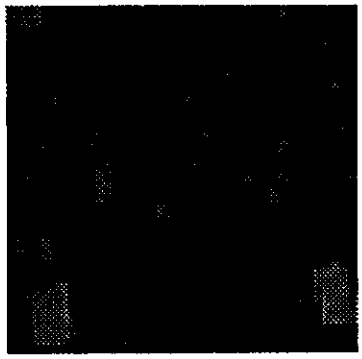

Figure (5a): Scene without air-craft
DSM = 188

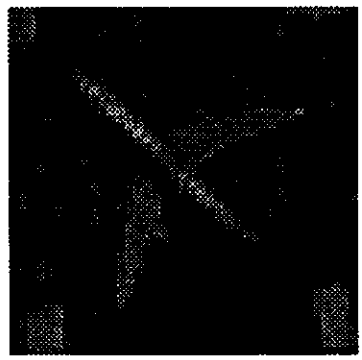

Figure (5b): Same scene of Figure (5a) with air-craft
DSM = 287

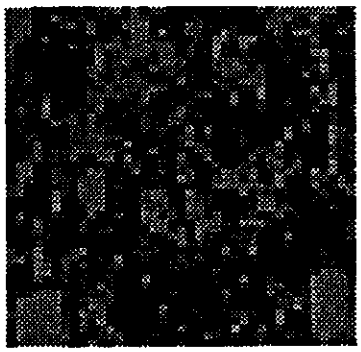

Figure (6a): Scene without air-craft
DSM = 34

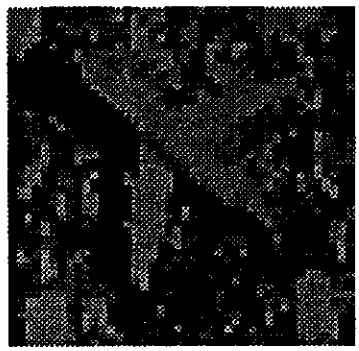

Figure (6b): Same scene of Figure (6a) with air-craft
DSM = 50

S. No.	Scene	DSM with Aircraft	DSM without Aircraft	Absolute Percent Change
1	Figure (3)	193	141	27
2	Figure (4)	195	151	22
3	Figure (5)	188	287	53
4	Figure (6)	34	50	47

Table 1: Summary of miniature aircraft results

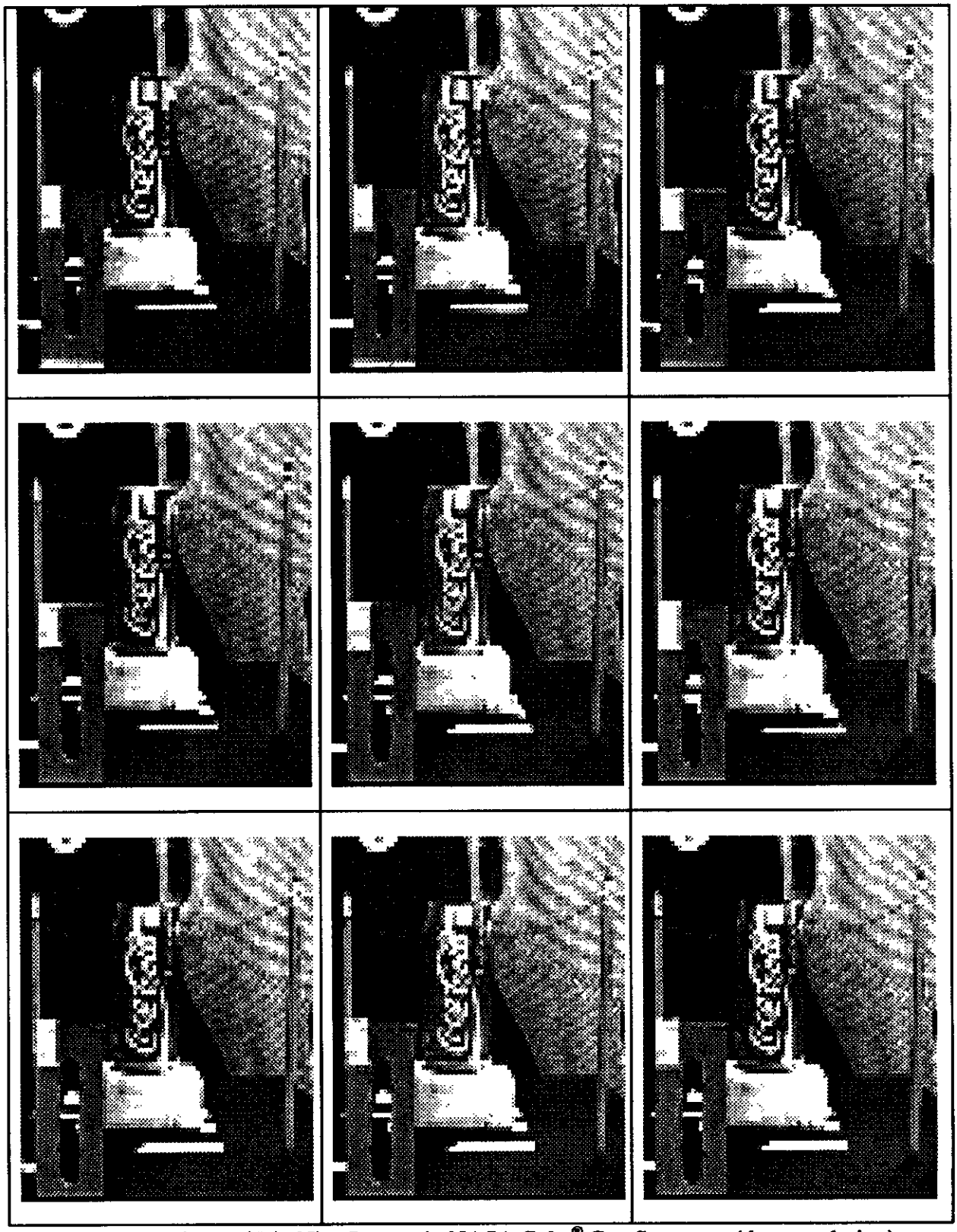

Figure (7a): Nine Images in NASA Coke® Can Sequence (low resolution)

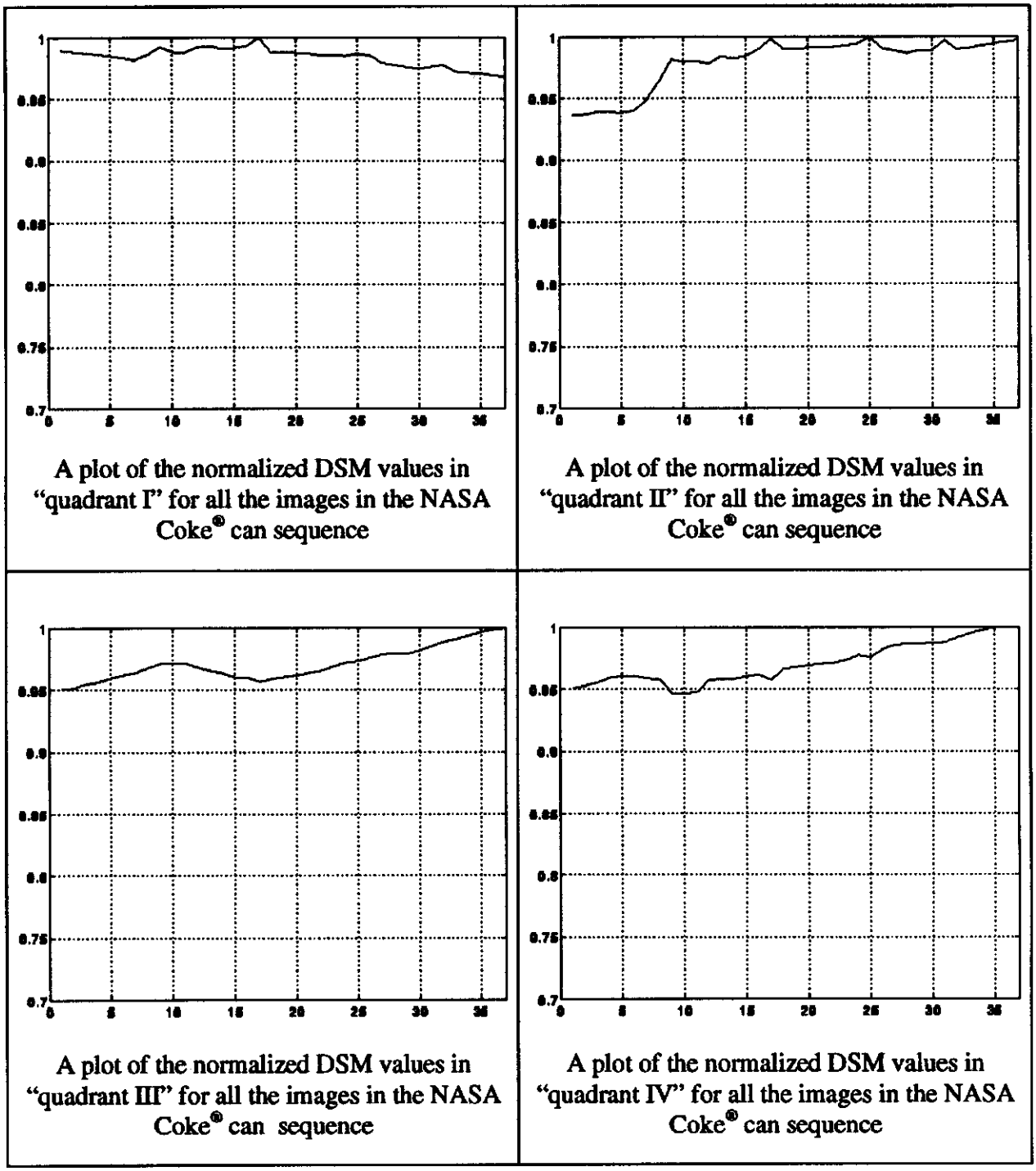

A plot of the normalized DSM values in "quadrant I" for all the images in the NASA Coke® can sequence

A plot of the normalized DSM values in "quadrant II" for all the images in the NASA Coke® can sequence

A plot of the normalized DSM values in "quadrant III" for all the images in the NASA Coke® can sequence

A plot of the normalized DSM values in "quadrant IV" for all the images in the NASA Coke® can sequence

Figure (7b): Plots of the normalized DSM values in four quadrants of the image, x-axis represents the image sequence number and the y-coordinate represents the corresponding DSM Value

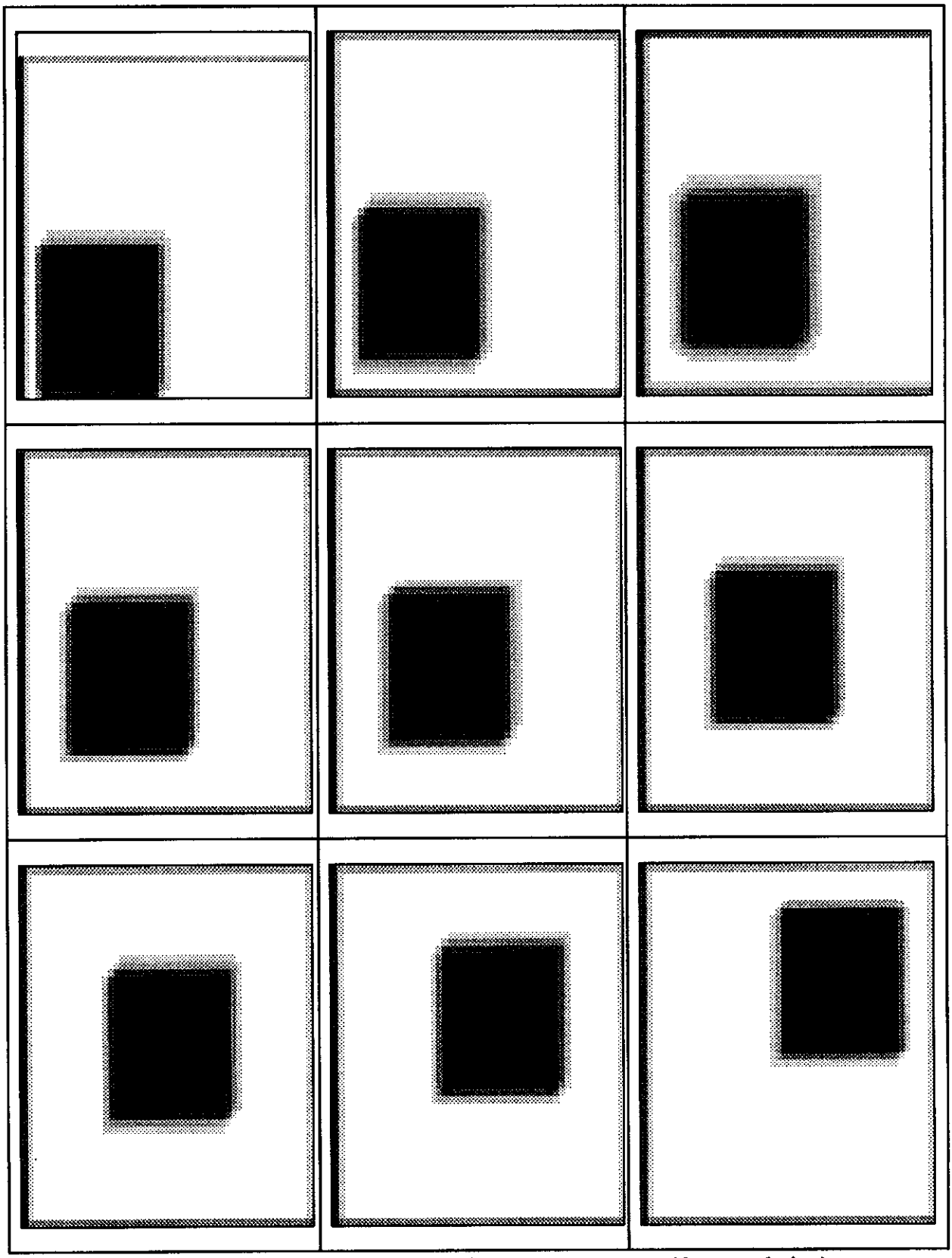

Figure (8a): Nine Images in a moving square sequence (low resolution)

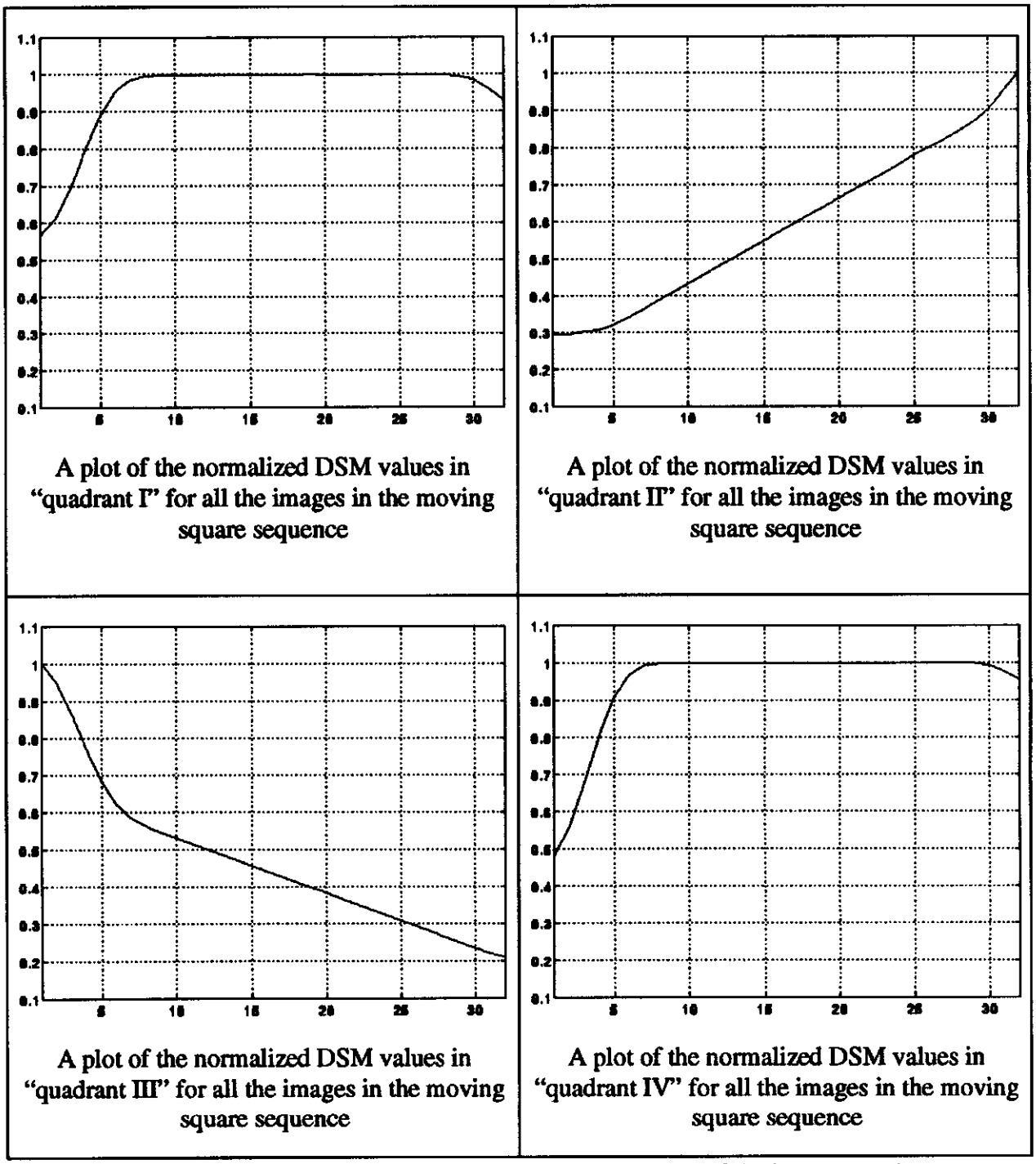

A plot of the normalized DSM values in "quadrant I" for all the images in the moving square sequence

A plot of the normalized DSM values in "quadrant II" for all the images in the moving square sequence

A plot of the normalized DSM values in "quadrant III" for all the images in the moving square sequence

A plot of the normalized DSM values in "quadrant IV" for all the images in the moving square sequence

Figure (8b): Plots of the normalized DSM in four quadrants of the image, x-axis represents the image sequence number and the y-coordinate represents the corresponding DSM Value

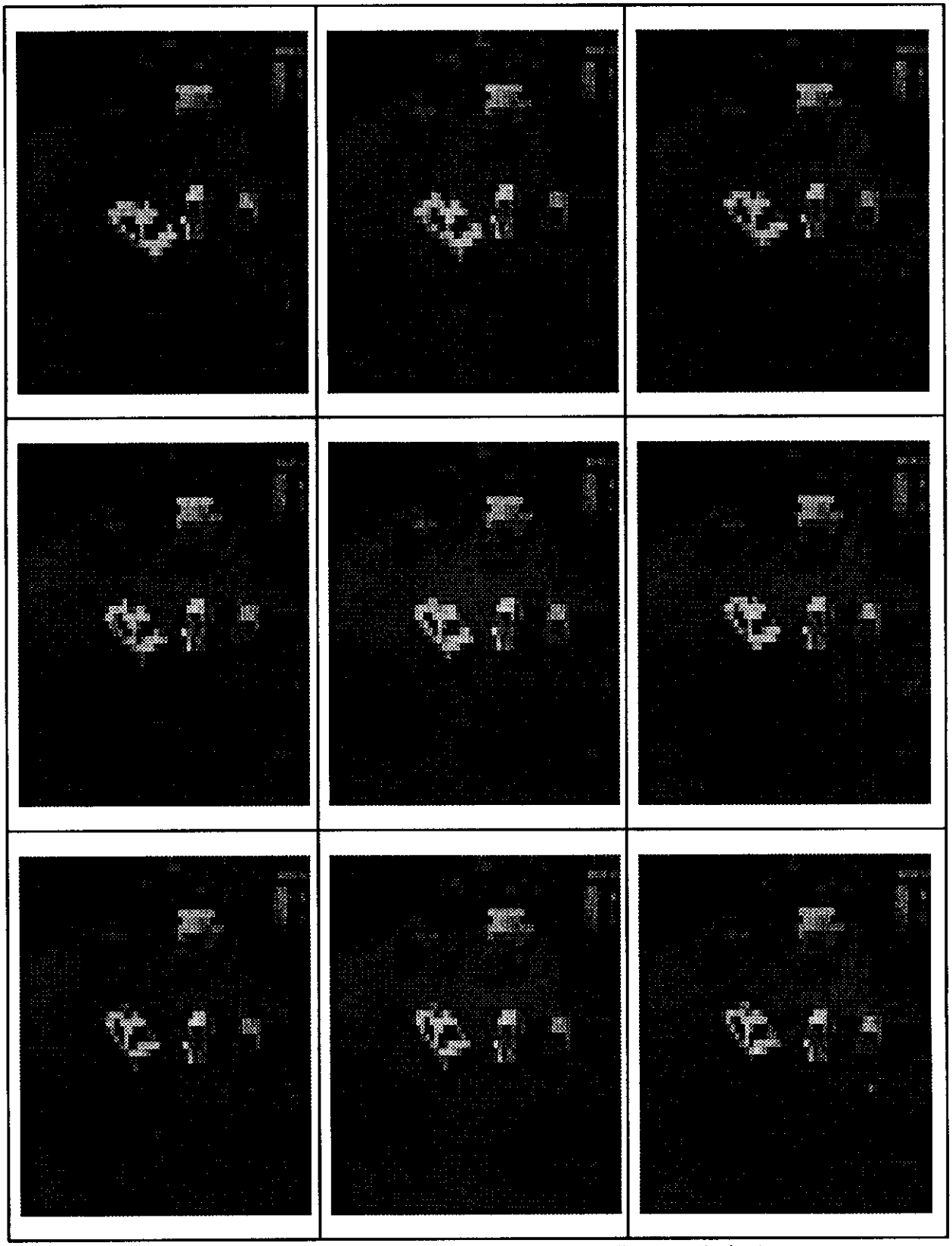

Figure (9a): Nine Images in Hamburg Taxi sequence (low resolution)

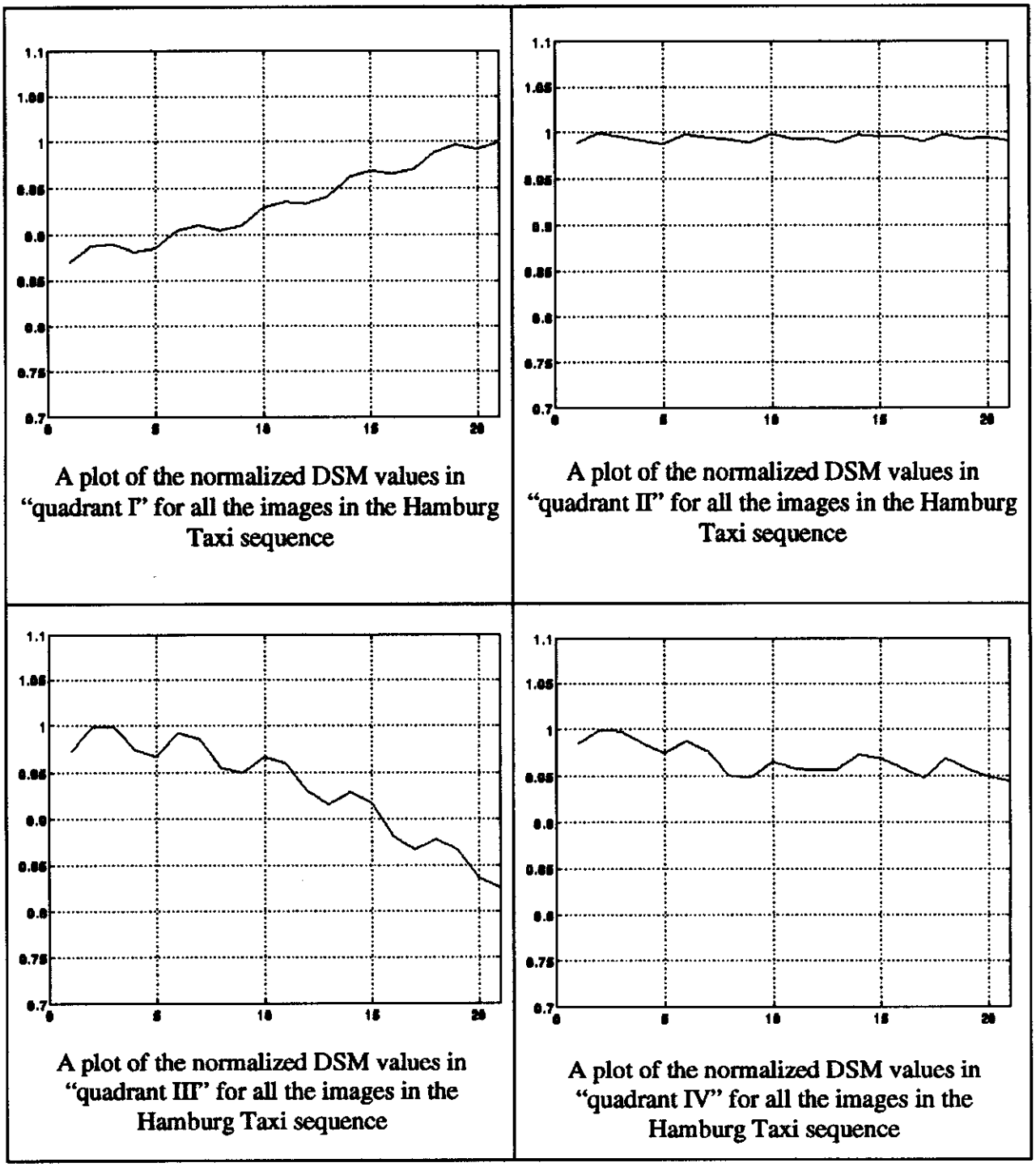

A plot of the normalized DSM values in "quadrant I" for all the images in the Hamburg Taxi sequence

A plot of the normalized DSM values in "quadrant II" for all the images in the Hamburg Taxi sequence

A plot of the normalized DSM values in "quadrant III" for all the images in the Hamburg Taxi sequence

A plot of the normalized DSM values in "quadrant IV" for all the images in the Hamburg Taxi sequence

Figure (9b): Plots of the normalized DSM in four quadrants of the image, x-axis represents the image sequence number and the y-coordinate represents the corresponding DSM Value

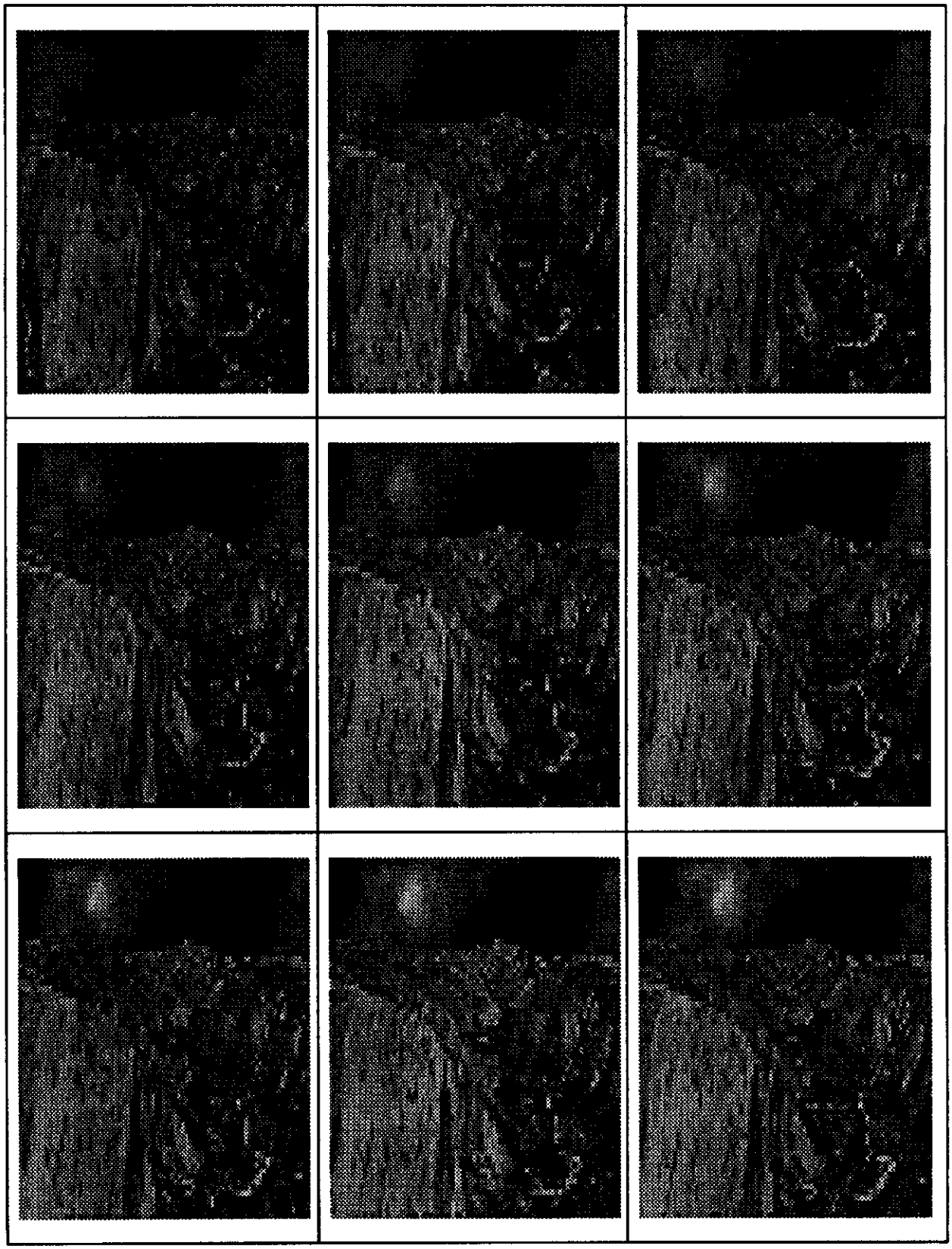

Figure (10a): Nine Images in Yosemite sequence (low resolution)

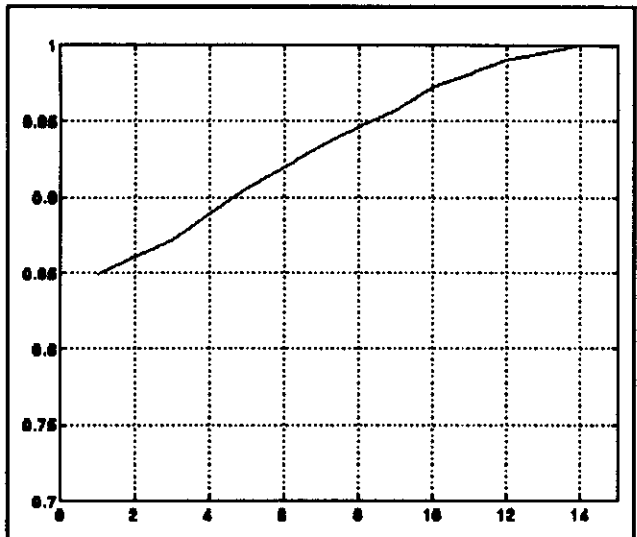

A plot of the normalized DSM values in "quadrant I" for all the images in the Yosemite sequence

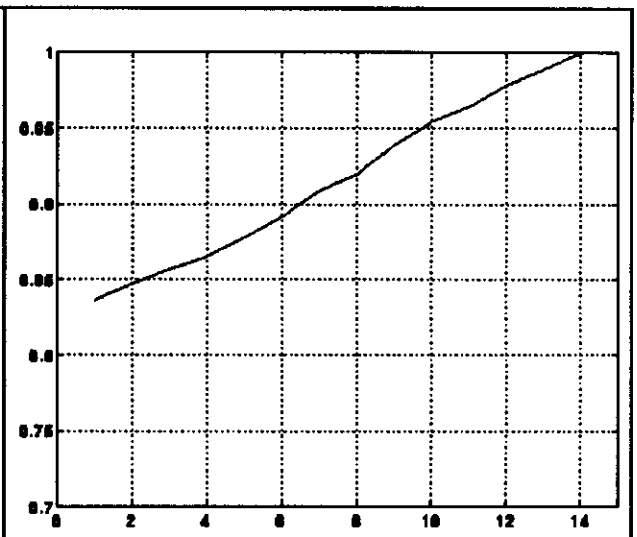

A plot of the normalized DSM values in "quadrant II" for all the images in the Yosemite sequence

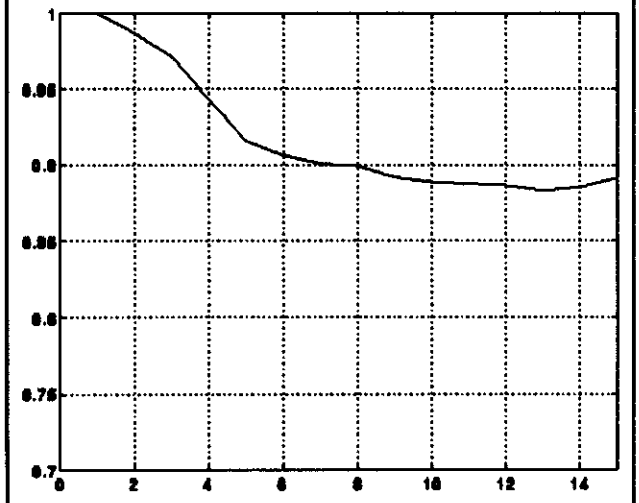

A plot of the normalized DSM values in "quadrant III" for all the images in the Yosemite sequence

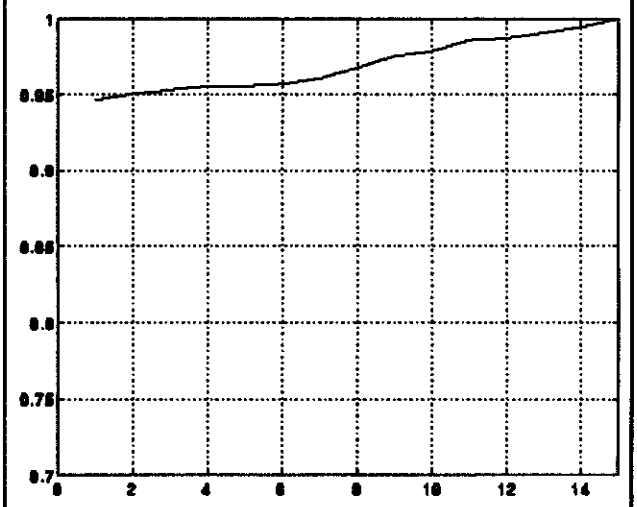

A plot of the normalized DSM values in "quadrant IV" for all the images in the Yosemite sequence

Figure (10b): Plots of the normalized DSM in four quadrants of the image, x-axis represents the image sequence number and the y-coordinate represents the corresponding DSM Value

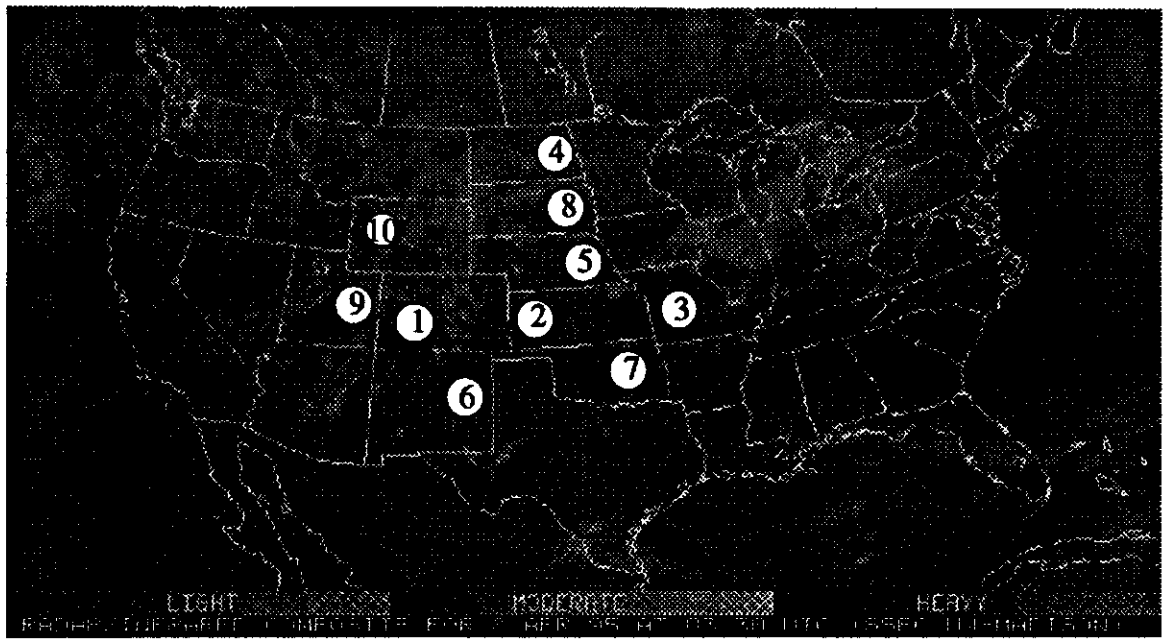

Figure (11a): Satellite Image of North America

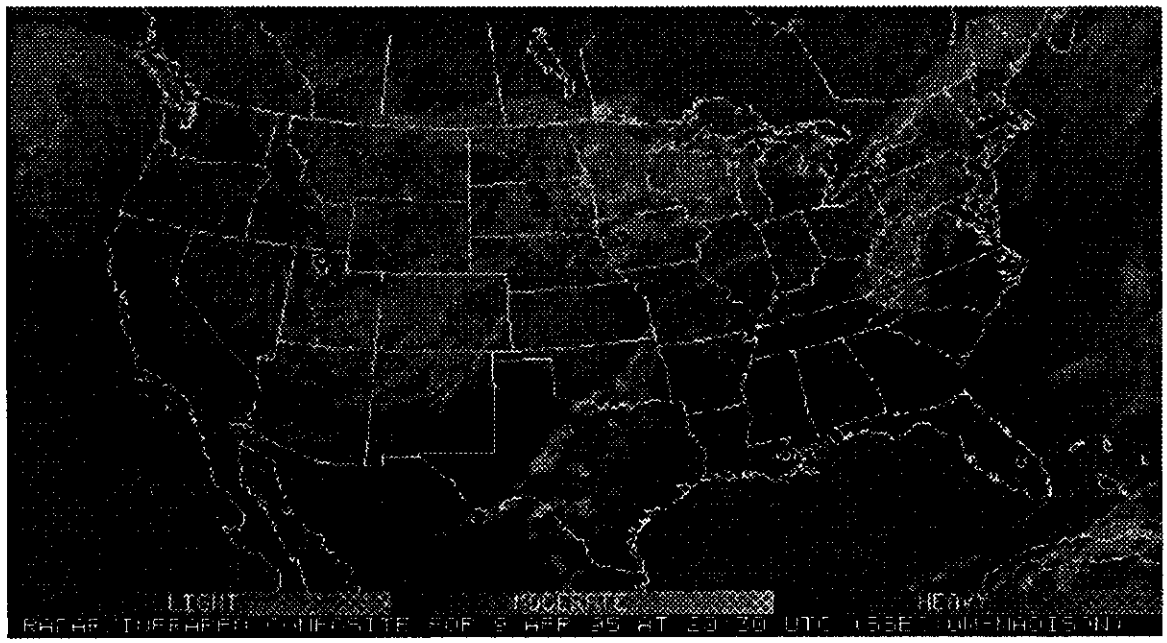

Figure (11b): Satellite Image of North America

S. No.	State	Region	DSM 1	DSM II	Percent Change
1a	Colorado	I	638	737	15
1b	Colorado	II	655	423	35
1c	Colorado	III	689	852	23
1d	Colorado	IV	678	571	16
2a	Kansas	I	472	2017	327
2b	Kansas	II	361	760	110
2c	Kansas	III	408	2067	407
2d	Kansas	IV	415	400	4
3a	Missouri	I	482	916	90
3b	Missouri	II	472	1378	191
3c	Missouri	III	156	691	342
3d	Missouri	IV	223	377	69
4a	N. Dakota	I	308	244	21
4b	N. Dakota	II	352	348	0.9
4c	N. Dakota	III	568	128	77
4d	N. Dakota	IV	241	265	10
5a	Nebraska	I	271	289	7
5b	Nebraska	II	432	394	9
5c	Nebraska	III	466	230	50
5d	Nebraska	IV	598	1005	68
6a	New Mexico	I	565	841	49
6b	New Mexico	II	853	2016	136
6c	New Mexico	III	532	747	40
6d	New Mexico	IV	557	989	77
7a	Oklahoma	I	800	856	7
7b	Oklahoma	II	921	513	44
7c	Oklahoma	III	930	1037	11
7d	Oklahoma	IV	957	475	50
8a	S. Dakota	I	740	479	35
8b	S. Dakota	II	614	547	11
8c	S. Dakota	III	406	265	34
8d	S. Dakota	IV	379	381	0.5
9a	Utah	I	110	344	210
9b	Utah	II	436	588	35
9c	Utah	III	525	497	5
9d	Utah	IV	521	676	30
10a	Wyoming	I	483	463	4
10b	Wyoming	II	604	363	40
10c	Wyoming	III	1476	1230	17
10d	Wyoming	IV	740	862	16

Table (2): Summary of cloud detection results

5 Machine Vision Applications of the DSM-Based Change Detection

The DSM-based change detection techniques described earlier can be used in many applications. In this section we outline a few applications.

1. Control of traffic employing traffic signals operating on a time basis constitutes an open-loop control system [14]. If somehow the presence or absence of cars in particular section(s) of the junction are detected and this information if relayed to the central computer system traffic jams in the city can be minimized. Traditionally, the presence or absence of vehicles at traffic junctions is detected by placing sensors beneath the road surface. The DSM algorithm described earlier can be used to detect the presence or absence of vehicles at a junction (see Appendix D). Based on the changes in the DSM value of a particular ROI the timing of the traffic signals can be changed, allowing more time for those sections of the junction where there are many cars.
2. In many industrial applications robots are used for manufacturing automation. Let us consider the task of packaging a finished product. Once a finished product arrives at a particular location then it has to be picked and placed in a packaging box. In such applications how does the robot know that the finished product has arrived? This can be achieved by visual monitoring of a particular ROI for the presence of the product. The DSM value of the ROI mentioned earlier can be used to detect the presence or absence of the product in the ROI.

3. Presence of materials such as glass, stone or metal in packaged food items is dangerous for consumers. X-ray imaging may used to image the contents of the finished packs [18]. Based on the changes in the DSM of the ROI it will be possible to detect contamination in food.
4. Robust detection of changes in images play a *crucial* role in Model Support Exploitation (MSE) Paradigm described in [16]. The MSE paradigm assumes that information about the scene and imaging parameters are assumed to be known a-priori: imaging conditions such as object orientation and position, geographic location, radiometric conditions such as the source of illumination, brightness, contrast, surface properties, functionality context such as airport, parking lot, etc. [16]. Given the above mentioned information about a scene to be monitored, detection of changes in such a scene may be used to trigger other events. The cause of the changes might be due to new construction, bomb damage, new construction etc. [16]. Several other applications of change detection algorithms in MSE are presented in [17]. The DSM mentioned earlier can be used in MSE.
5. It can be used in detecting the presence or absence of a vehicle in a parking lot. This information may be used to implement a vision-based parking meter (see Appendix E).
6. With some a-priori knowledge about the ROI it may be possible to predict weather conditions of the ROI autonomously.
7. The DSM can be used in monitoring changes on the earth namely urban developments, vegetation flood monitoring, deforestation, etc.
8. In many defense applications such as border surveillance for encroachments, etc.

In addition to the applications mentioned here, there are several such areas where several events can be triggered based on changes in the images. The key information in all such applications is the detection of changes from one image to another.

7 Conclusions

This paper presents a new approach for change detection based on the dissimilarity measure of the ROI in an image. This algorithm needs no a-priori knowledge about the scene. It does not need to know the sensor position and orientation and camera parameters like focal length, aperture etc. Slow changes in intensity as well as sensor location and orientation can be tolerated since they do not cause abrupt temporal changes in the value of the DSM. Several dissimilarity measures for the ROI in the image are presented. However, due to simplicity we have employed the DSM based on the city block metric through out this paper. Currently we are investigating the performance of the other dissimilarity measures outlined here as change detection criteria in various machine vision applications.

Acknowledgments

The authors would like to thank Dr. Barron, Dr. Fleet and Dr. Beauchemin of Queens University, Canada, for providing us with the synthetic image sequences used in the study.

References

[1] R. Chellapa, Q. Zheng, L. S. Davis, C. L. Lin, X. Zhang, C. Rodriguez, A. Rosenfeld and T. Moore (1994), "Site-Model-Based Monitoring of Aerial Images," *Proc. Image Understanding Workshop*, pp. 295-318.

[2] J. Wiklund and G. H. Granlund (1987), "Image Sequence Analysis for Object Tracking," *Proc. 5th. Scandinavian Conf. on Image Analysis*, Stockholm, pp. 641-48.

[3] G. W. Donohoe, D. R. Hush and N. Ahmed (1988), "Change Detection for Target Detection and Classification in Video Sequences," *Proc. Int'l Conf. Acoustics, Speech Signal Proc.*, New York, pp. 1084-87.

[4] R. Gonzalez and P. Wintz (1987), *Digital Image Processing*, Addison-Wesley.

[5] D. N. Hein and N. Ahmed (1981), "Video Compression Using Conditional Replenishment and Motion Prediction," *IEEE Trans. Electromagnetic Compatibility*, Vol. EMC-26, pp. 134-42.

[6] G. Donohoe (1987), "Change Detection for Classification - A Summary," *Memo to the Signal Processing Lab*, Univ. of New Mexico, Albuquereque, NM.

[7] L Bryan and J. Clark (1984), "Potential for Change Detection using Seasat SAR data," *Remote Sensing of Environment*, Vol. 16, pp. 107-24.

[8] R. Lillestrand (1972), "Techniques for Change Detection," *IEEE Trans. on Computers*, Vol. C-21, No. 7, pp. 654-59.

[9] L Milstein and T. Lazicky (1978), "Statistical Test for Image Tracking," *Computer Graphics and Image Processing*, Vol. 7, pp. 413-24.

[10] R. M. Gagliardi, I. S. Reed, H. M. Shao and A. Margalit (1983), "Optical Target Detection using Dual Scene Observation," University of Southern California, *EE Report.*

[11] A. Margalit, I. S. Reed and R. M. Gagliardi (1985), "Adaptive Optical Target Detection Using Correlated Images," *IEEE Trans. on Aerospace Electr. Systems*, Vol. AES-21, No. 3, pp. 394-405.

[12] T. Fung and E. LeDrew (1987), "Application of Principal Component Analysis to Change Detection," *Photogrammetric Engineering and Remote Sensing*, Vol, 53, No. 12, pp. 1649-58.

[13] J. L. Mundy and P. Vrobel (1994), "The Role of IU Technology in RADIUS phase II," *Proc. Image Understanding Workshop 1994*, University of California at Riverside, pp. 251-64.

[14] K. Ogata (1990), *Modern Control Engineering*, Prentice Hall Inc, New Jersey, USA.

[15] K. I. Laws (1979), "Texture Energy Measures," *Proc. of Image Understanding Workshop*, pp. 47-51.

[16] A. Hoogs and D. Hackett (1994), "Model Support Exploitation as a Frame Work for Image Understanding," *Proc. Image Understanding Workshop 1994*, University of California at Riverside, pp. 265-68.

[17] T. M. Strat and W. D. Climeson (1994), "RADIUS: Site Model Content," *Proc. Image Understanding Workshop 1994*, University of California at Riverside, pp. 277-85.

[18] D. Patel, I. Hannah and E. R. Davies (1994), "Foreign Object Detection via Texture Analysis," *Proc. of Intl. conf. on Pattern Recognition*, Jerusalem, Israel, pp. 586-88.

[19] H. C. Romesburg (1990), *Clustering Analysis for Researchers*, Robert E. Krieger Publishing Company, Malabar, FL.

[20] J. L Barron, D. J. Fleet and S. S. Beauchemin (1992), "Performance of Optical Flow Techniques," *RPL-TR-9107*, Dept. of Computing and Information Science, Queens University, Canada.

[21] D. J. Gerson and S. E. Wood, Jr. (1994), "RADIUS Phase II The RADIUS Testbed System," *Proc. Image Understanding Workshop*, pp. 231-37.

[22] L. Kaufman and P. J. Rousseeuw (1990), *Finding Groups in Data: An Introduction to Cluster Analysis*, John Wiley & Sons Inc., New York.

[23] S. Kullback (1968), *Information Theory and Statistics*, Dover Publications, New York.

Appendix A: Dissimilarity Measure (DSM) of Images

Let (x,y) be the spatial coordinates of an arbitrary pixel in the image, where x, y are integers and I(x,y) be the intensity at (x, y). The inter-pixel distance is denoted by δ and is defined as follows.

$$\delta = (\Delta x, \Delta y) \tag{A1}$$

where Δx = difference between the corresponding x coordinates of two pixels; Δy = difference between the corresponding y coordinates of two pixels.

The dissimilarity between the image intensities of pixels separated by the inter-pixel distance defined in Equation (B1) can be characterized by the City Block Metric (CBM), which is defined as [22]:

$$CBM = \{|I(x,y) - I(x+\Delta x, y+\Delta y)|\} \tag{A2}$$

where I(x,y) = intensity at pixel (x,y); I(x+Δx, y+Δy) = intensity at pixel (x+ΔX, y+Δy).

Several other dissimilarity measures may be used instead of the one used in Equation (B2). A detailed description of these measures is presented in (see Appendix B).

Each pixel (x,y) in an image can be characterized by a matrix known dissimilarity matrix, which is basically a matrix of numbers that characterizes the dissimilarity of pixel intensities in the neighborhood of the pixel. For instance, if the texture is smooth, the dissimilarity is very low, hence the mean value of the dissimilarity matrix is low. This dissimilarity matrix is a (2Lr+1)X(2Lc+1), where Lc, Lr are positive integer constants. The (i,j) element of this matrix is the CBM defined in Equation (B2), i = -Lc, ...,-1,0,1,...Lc and j = -Lr,...,-1,0,1,...,Lr. The (0,0) element of the dissimilarity matrix is zero since {|I(x,y)-I(x+0,y+0)}| = 0. A matrix of numbers can be generated for any pixel.

This dissimilarity matrix can be used to generate a global image variable to indicate the smoothness of texture details in an image. Next we show how to generate a global measure which indicates the texture smoothness.

We select an arbitrary window in the image plane. Let x_i and x_f be the initial and final coordinates of the window along the x-direction respectively and y_i and y_f be the initial and final coordinates of the window along the y-direction respectively. For each pixel in the window selected we compute the sum of all elements in the dissimilarity matrix described above. Thus there are $(x_f-x_i)X(y_i-y_f)$ sums for the window selected, i.e., mathematically it can be described as follows.

$$DSM = \sum_{x=x_i}^{x_f} \sum_{y=y_i}^{y_f} \left(\sum_{p=-L_c}^{L_c} \sum_{q=-L_r}^{L_r} |I(x,y) - I(x+p, y+q)| \right) \qquad \text{(A3)}$$

Where I(x,y) is the intensity at pixel (x,y) and x_i and x_f are the initial and final x-coordinates of the window respectively ; y_i and y_f are the initial and final y-coordinates of the window in the image respectively and Lc and Lr are positive integer constants, need not be equal.

Appendix B: Alternative Dissimilarity Measures

In this section we present several other dissimilarity measures based on various distance metrics. They are as follows:

a) Minkowski Metric Based DSM (MDSM)

We define the image DSM based on the Minkowski metric as follows:

$$MDSM = k\sum_{x=x_i}^{x_f}\sum_{y=y_i}^{y_f}\left(\left(\sum_{p=-L_c}^{L_c}\sum_{q=-L_r}^{L_r}|I(x,y)-I(x+p,y+q)|^r\right)^{\frac{1}{r}}\right)$$

where I(x,y) is the intensity at pixel (x,y) and x_i and x_f are the initial and final x-coordinates of the window respectively ; y_i and y_f are the initial and final y-coordinates of the window in the image respectively and Lc and Lr are positive integer constants, need not be equal. r is a positive integer. If r = 1, we get the City Block Metric. If r = 2, we obtain the Euclidean metric. k is a positive constant dependent upon the Lc, Lr, x_i, x_f, y_i, y_f and the maximum value of the intensity level. For change detection purposes as mentioned earlier we are not interested in the absolute value of the DSM but we are interested in the changes.

b) Kullback DSM (KDSM)

We define the image DSM based on Kullback measure [23] as follows as follows:

$$KDSM = k\sum_{x=x_i}^{x_f}\sum_{y=y_i}^{y_f}\left(\sum_{p=-L_c}^{L_c}\sum_{q=-L_r}^{L_r}(I(x,y)-I(x+p,y+q))\log\left(\frac{I(x,y)+\varepsilon}{I(x+p,y+q)+\varepsilon}\right)\right)$$

where I(x,y) is the intensity at pixel (x,y) and x_i and x_f are the initial and final x-coordinates of the window respectively ; y_i and y_f are the initial and final y-coordinates of

the window in the image respectively and Lc and Lr are positive integer constants, need not be equal. k is some positive constant.

c) Minkowski Metric Based DSM1 (MDSM1)

This is a modified Minkowski Metric Based DSM. It is useful in images corrupted with noise.

$$MDSM1 = k\sum_{x=x_i}^{x_f}\sum_{y=y_i}^{y_f}\left(\left(\sum_{p=-L_c}^{L_c}\sum_{q=-L_r}^{L_r}\left|I(x+p,y+q)-\frac{1}{(2L_c+1)(2L_r+1)}\sum_{p=-L_c}^{L_c}\sum_{q=-L_r}^{L_r}I(x+p,y+q)\right|^r\right)^{\frac{1}{r}}\right)$$

where I(x,y) is the intensity at pixel (x,y) and x_i and x_f are the initial and final x-coordinates of the window respectively ; y_i and y_f are the initial and final y-coordinates of the window in the image respectively and Lc and Lr are positive integer constants, need not be equal. r is a positive integer, k is a positive constant dependent upon the Lc, Lr, x_i, x_f, y_i, y_f and the maximum value of the intensity level.

d) Kullback DSM1 (KDSM1)

This is a modified KDSM described above. This metric is suitable for images corrupted by noise.

$$KDSM1 = k\sum_{x=x_i}^{x_f}\sum_{y=y_i}^{y_f}\left(\sum_{p=-L_c}^{L_c}\sum_{q=-L_r}^{L_r}(I(x+p,y+q)-\mu)\log\left(\frac{I(x+p,y+q)+\varepsilon}{\mu+\varepsilon}\right)\right)$$

$$\mu = \sum_{p=-L_c}^{L_c}\sum_{q=-L_r}^{L_r}I(x+p,y+q)$$

where I(x,y) is the intensity at pixel (x,y) and x_i and x_f are the initial and final x-coordinates of the window respectively ; y_i and y_f are the initial and final y-coordinates of the window in the image respectively and Lc and Lr are positive integer constants, need not be equal. k is some positive constant.

Appendix C: Subtraction Vs. DSM

One of the conventional approaches used in the area of change detection is image differencing. In this section we present a comparison of the image differencing technique for change detection versus the DSM criterion for change detection.

An image from the Yosemite sequence (Figure (9a)) is used in this study. From this image we generated four different images. Each image is obtained by shifting the original image by one, two three and four pixels. For these images we computed the DSM values and they are summarized in Table (C1). Also we computed the differences in the images When there is no shift the mean value of the difference between the images is zero. When there is a shift of one pixel the mean value is no longer zero. The results are summarized in Table (C3).

The magnitude of numbers in Table (C1) as well as Table (C3) have no meaning but the changes in their values play an in important role in change detection. We compared the percent changes in these values when there is a shift of image intensities. The results are summarized in Tables (C1-C4). Tables (C5-C7) present a comparison of relative variations of the DSM values against the corresponding changes in the image difference for various pixel shifts

From Tables (C5-C7) it is clear that a small shift in gray level intensity results in a very large relative variations in the image difference where as the relative variations in the DSM values are very small.

S. No.	Quadrant	DSM of Original Image	DSM of the Image Shifted by one Pixel to the right	DSM of the Image Shifted by two Pixels to the right	DSM of the Image Shifted by three Pixels to the right	DSM of the Image Shifted by four Pixels to the right
1	I	254497	254690	255011	255499	256196
2	II	310928	310553	310188	309745	309125
3	III	337397	340873	341024	340777	340275
4	IV	515368	516657	517594	518513	519660

Table (C1): Summary of the DSM for shifted images

S. No	Quadrant	$\left\|\frac{\Delta DSM}{DSM}\right\|$ from one pixel to two pixel shift	$\left\|\frac{\Delta DSM}{DSM}\right\|$ from two pixels to three pixels shift	$\left\|\frac{\Delta DSM}{DSM}\right\|$ from three pixels to four pixels shift
1	I	0.126	0.19	0.273
2	II	0.118	0.15	0.2
3	III	0.275	0.073	0.147
4	IV	0.181	0.177	0.221

Table (C2): Summary of Percentage Changes for the results presented in Table (C1)

S. No.	Quadrant	Actual Value (In the absence of any shift)	Value obtained due to Image Shifted by one Pixel to the right	Value obtained due to Image Shifted by two Pixels to the right	Value obtained due to Image Shifted by three Pixels to the right	Value obtained due to Image Shifted by four Pixels to the right
1	I	0	98423	157803	198193	229391
2	II	0	133467	219113	271965	307433
3	III	0	223132	339574	398738	436422
4	IV	0	276732	408084	480444	528232

Table (C3): Summary of Image Subtraction for shifted images

S. No.	Quadrant	Percent change from one pixel to two pixel shift (absolute)	Percent change from two pixels to three pixels shift (absolute)	Percent change from three pixels to four pixels shift (absolute)
1	I	60	26	16
2	II	64	24	13
3	III	53	17	10
4	IV	47	18	10

Table (C4): Summary of Percentage Changes for the results presented in Table (C3)

S. No	Quadrant	$\left\lvert\frac{\Delta DSM}{DSM}\right\rvert$ from one pixel to two pixel shift	Percent change from one pixel to two pixel shift (absolute)
1	I	0.126	60
2	II	0.118	64
3	III	0.275	53
4	IV	0.181	47

Table (C5): Comparison of relative changes in the DSM and the relative changes in the image difference for one pixel to two pixel shift in the image intensity.

S. No	Quadrant	$\left\lvert\frac{\Delta DSM}{DSM}\right\rvert$ from two pixels to three pixels shift	Percent change from two pixels to three pixels shift (absolute)
1	I	0.19	26
2	II	0.15	24
3	III	0.073	17
4	IV	0.177	18

Table (C6): Comparison of relative changes in the DSM and the relative changes in the image difference for two pixels to three pixels shift in the image intensity.

S. No	Quadrant	$\left\lvert\frac{\Delta DSM}{DSM}\right\rvert$ from three pixels to four pixels shift	Percent change from three pixels to four pixels shift (absolute)
1	I	0.273	16
2	II	0.2	13
3	III	0.147	10
4	IV	0.221	10

Table (C7): Comparison of relative changes in the DSM and the relative changes in the image difference for three pixels to four pixels shift in the image intensity.

Appendix D: Vision-Based Traffic Control System

A potential application of the DSM mentioned earlier is a vision-based traffic controller that constantly monitors a traffic junction (see Figures (D1) and (D2)). Depending upon the changes in the DSM value in the images the timing of the green signal can be adjusted, i.e., there is a scope for an intelligent system to adjust the time allowed for a green signal depending upon the occupancy of the regions identified on the road.

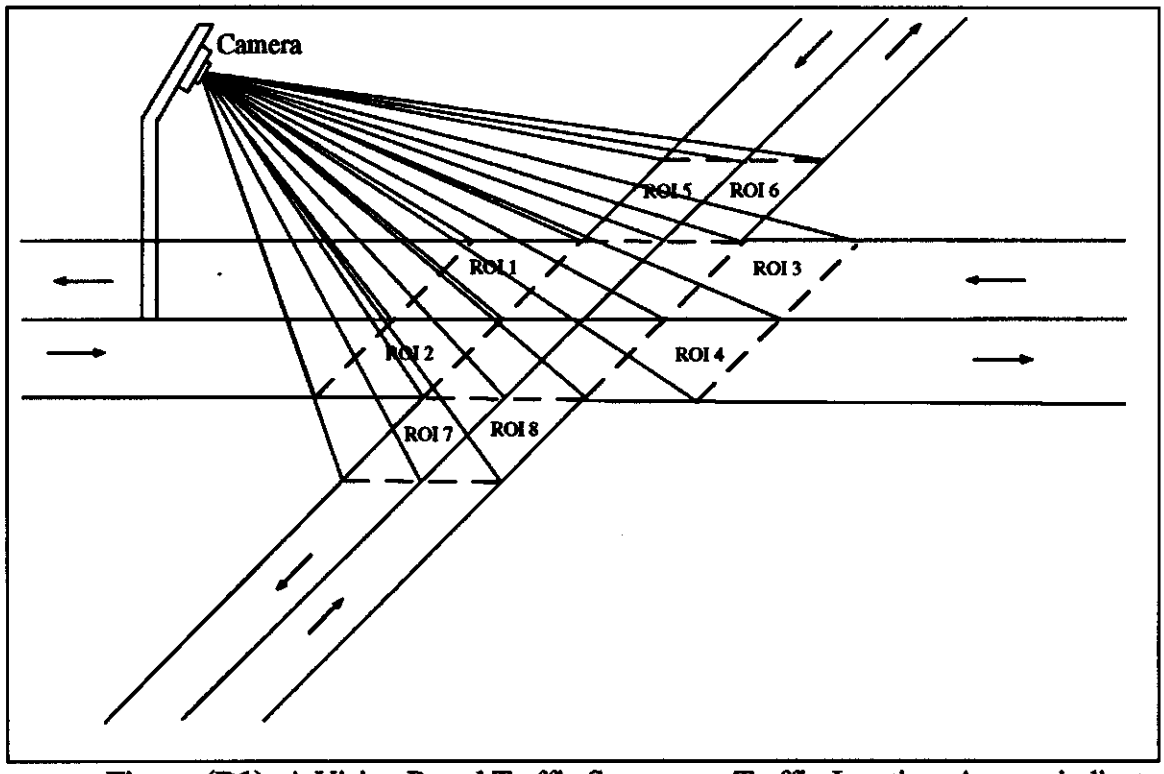

Figure (D1): A Vision Based Traffic Sensor at a Traffic Junction, Arrows indicate the direction of Traffic

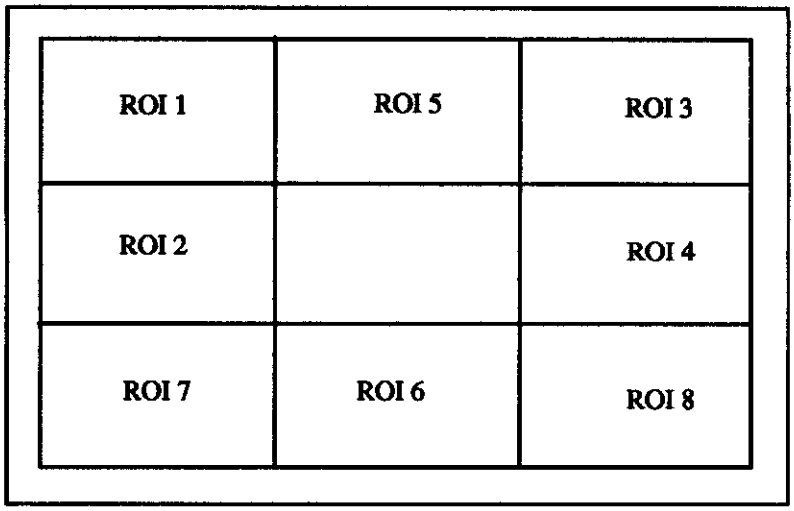

Figure (D2): Corresponding Regions of the road in the Image

Appendix E: An Image-Based Parking Meter

We present an idea of using the DSM described earlier to be used as sensory information in a vision-based parking meter. Consider a vision-based parking meter. It is desired to start the meter as soon as the vehicle enters the parking lot and reset the meter as soon as the vehicle leaves the lot, and also indicate a warning signal if the vehicle exceeds the prescribed time. Several issues need to be addressed to be addressed in such a system. The main concern is how to detect the presence or absence of vehicle. The DSM described in this report can be used to detect the presence or absence of the vehicle in the lot. If the system constantly monitors the parking lot (see Figures (E1) and (E2)), the desired task of detecting the presence or absence of the vehicle in the lot can be achieved. As shown in Appendix C there won't be a change in DSM value after the vehicle enters the monitored area as opposed to the subtraction algorithms which may detect huge changes when the vehicle tries to align between the lane marks.

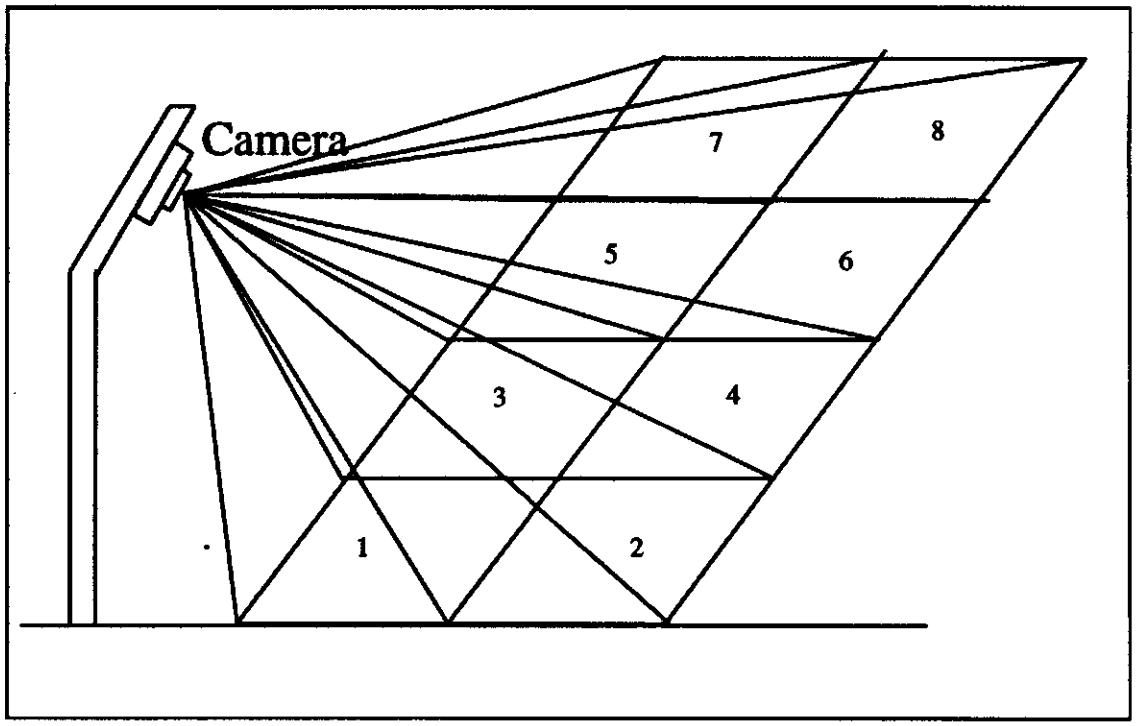

Figure (E1): Camera monitoring a Parking Lot

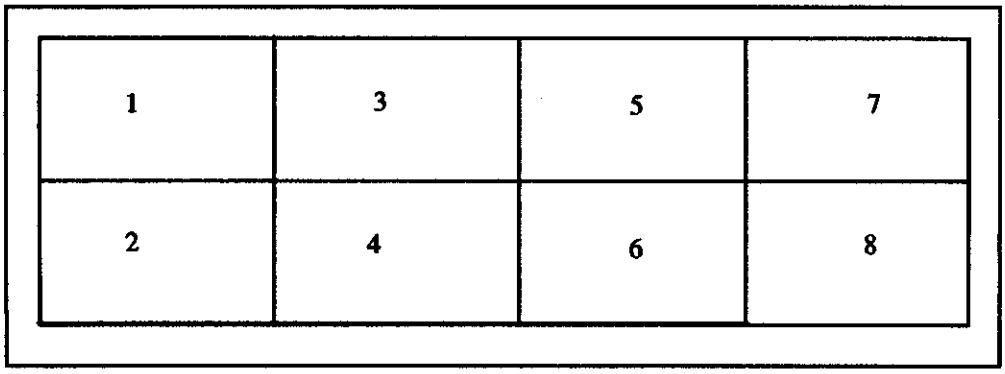

Figure (E2): Corresponding Image